Proceedings of the joint ICVRAM ISUMA UNCERTAINTIES conference
Florianopolis, SC, Brazil, April 8-11, 2018

Applying Kalman Filtering to Unbalance Estimation in Rotating Machinery

Miguel A. C. Michalski[1], **Gilberto F. M. de Souza**[1]

[1] Escola Politécnica – Universidade de São Paulo, Av. Prof. Mello Moraes, 2231– Cidade Universitária, São Paulo-SP
michalski@usp.br
gfmsouza@usp.br

Keywords. Kalman Filtering, Monte Carlo Method, Finite Element Method, Unbalance, Rotating Machinery

Abstract. The use of monitoring systems for rotating machinery diagnosis brings, with no doubt, great benefits to the industry in general. This is not different in electric power generation plants. The reliability currently achieved in turbines and generators operation is already considerably high, although there is still a driver for shorter shutdown times and reducing non-scheduled shutdowns to zero, therefore, allowing the longest possible operating time for such equipment. In this way, it remains a challenge for research and industry to develop better monitoring, diagnosis and prognostic techniques. When such a development is carried out only in the laboratory, several issues remain open when transferring the new techniques to industry, or the so-called "real world". In other hand, hardly a large equipment is available for faults inserts and subsequent analysis in powerplants. Hence, computational modeling of rotating machines becomes practically the only way out, with all the models' inherent uncertainties and the noise related to the few data acquired. This way, algorithms used to model and estimate these faults, even the simplest ones like unbalance, must consider such uncertainties. The Kalman filter, for example, is one of the methods that can bring a light on the results of this process. Therefore, the objective of this paper is to present some initial results in the unbalance estimation in rotating machines using this method. Some rotors were selected as examples, including a laboratory test rig and a turbocharger used in the petrochemical industry. Actual data and computer simulations were used to validate the method and to provide the unbalance estimation of the selected machines.

1 INTRODUCTION

Considering the evolution of the mechanical maintenance in the last decades, it is notorious how its role has changed, particularly in power generation companies. In practice, with the use of modern maintenance techniques, as predictive maintenance and reliability centered maintenance (RCM), maintenance is no longer understood as "the way to keep the integrity of a physical asset" and became to be understood as "the way to keep a physical asset operational with the maximum level of reliability". In fact, considering RCM principles, maintenance is focused is the system functions, and not the system hardware (Rausand, 1998) and can be understood as the process used to determine what must be done to ensure that any physical component continues to do whatever it was designed to do under the existing circumstances (Deepak Prabhakar and Jagathy Raj, 2014).

In fact, the crescent electricity demand, the changes in the way energy is traded in the Brazilian market and the adoption of modern equipment and renewable power (such as wind power) in the generation sector have led power generation companies to change maintenance philosophy and look for modern maintenance methods and tools. Not only in the national market, but also in the international scenario, the search for new technologies that allow a more efficient and accurate diagnosis is a reality. The maintenance requirements of offshore wind turbines in the North Sea and in countries such as Belgium, the Netherlands and England are an example of such demand.

Nowadays it is common to consider aspects related to the reliability and maintenance of equipment still in its design phase. Nevertheless, it was with the computational technological development that the major changes occurred. New maintenance management methodologies have been applied, from operational condition monitoring techniques to decision support tools and risk analysis. The use of techniques such as FMEA, expert systems, neural networks, nebulous logic, among other artificial intelligence techniques, becomes increasingly common.

In order to integrate all these information sources into a unique and comprehensive computational solution, integrated equipment health management systems can be considered. It would not be a mistake, therefore, to think of the integration of machines' diagnostic and prognostic algorithms in such systems (Walker, Perinpanayagam and Jennions, 2013). Some improvements would be achieved with such integration, such as safety increase through the use of diagnostics and prognostics to mitigate defects before they cause major damages or become a failure, availability growth through better maintenance scheduling, reliability improvement through a more complete understanding of the system health and the use of prognostic based maintenance and total maintenance cost reduction with unnecessary maintenance and unscheduled machine downtime decrement.

The condition monitoring of a rotary machine has progressed for many years with significant improvements, mainly based on data analysis and signal processing algorithms. Pattern recognition methods are well established and can successfully detect and classify various types of failures.

Some faults, however, are difficult to distinguish, and their quantification and location may require a significant number of tests, which can be time-consuming, costly, or even impossible to perform with simple field experiments. Therefore, a machine spatial model becomes necessary, as well as the application of methods to identify several parameters. The model accuracy will depend on its application and the intrinsic uncertainties issue can be solved, for example, with statistical methods.

In relation to data acquisition, practice for many years has been to collect data from the machines during rundowns or during the operating condition on load. In the first case, the data is rich in information, since the machine can be exciting while going through its critical speeds. In the second case, although the wealth of information is not large, there is a large amount of data. In this paper, the first case will be used.

Based on the works of Musynska (2005) and Bently and Hatch (2002), eight basic faults in rotating machines can be considered: unbalance, misalignment (linear and angular), wear and clearance, fluid induced instabilities, cracks in shafts, blades and vanes and, finally, shaft bows. Among them, three faults stand out and present common symptoms, mainly in the initial phase of degradation: unbalance, misalignment and shaft bows.

Although some authors present studies seeking to define the most common fault causes in rotary machines Walker, Perinpanayagam and Jennions (2013) emphasizes that due the lack of commercial information, it is very difficult to quantify the rate of each failure occurrence in a general way. However, there is a common sense that between these faults, unbalance is the most common fault found in rotors, since every rotating machine has an inherent degree of unbalance. In fact, it is practically impossible to manufacture a component that is perfectly balanced. The degree to which the unbalance affects the machining operation determines the problem extension (Silva, 2005).

Unbalance occurs synchronously in relation to machine rotation and is not necessarily a factor that leads to equipment damage or failure. Still, faults that may occur subsequently can cause damage and lead to equipment failure. As new frequency components arise with such faults combination, the unbalance location and its prognosis stay as a limited area of investigation.

Thus, as part of a larger project and still, a work in progress, the objective of this paper is to present some initial results in the unbalance estimation in rotating machines based on a Kalman Filter. Some strong assumptions will be taken and only the amount of unbalance will be estimated. Two different horizontal rotating machinery are considered: a laboratory test rig and a turbocharger used in the petrochemical industry.

At first, all the parameters of both systems will be considered known and the unbalance estimation will be performed. In a second moment, the bearings stiffness and damping of the chosen units will be considered random variables and their uncertainties will be propagated for the unbalance estimation with the Monte Carlo Method (MCM), similarly to a Monte Carlo Kalman Filter (Haug, 2012). The discretization of the mathematical models of each unit was done through the Finite Element Method (FEM).

Considering the paper workflow, the theoretical background and some basic assumptions will be presented next. In section three will be presented some considerations about the test rig and the turbocharger. Then, in section four are presented the results, along with some related discussion. Finally, in section five, the work conclusions are presented.

2 THEORETICAL BACKGROUND AND BASIC ASSUMPTIONS

The fundamental point to understand the presented method is the flexible rotor modelling, widely found in the literature in detail (Michalski, 2004). Basically, the structure of a flexible rotor can be subdivided into three fundamental components: the disk, modeled as a rigid body, being largely responsible for the system kinetic energy; the shaft, modeled as a flexible element, discretized and analyzed by the Finite Element Method, responsible for both the system kinetic and the potential energies; the bearings, discrete support elements with their stiffness and damping properties, contributing with the system potential energy and energy dissipation.

Initially considering the shaft, each of its discretized elements is represented by a Timoshenko beam element, having two nodes with four degrees of freedom each (two rotations and two translations, already assuming that there is no displacement in the axial direction and that the rotation around this axis is constant), totaling eight degrees of freedom per element. In each node, the disks and bearings elements are placed, contributing respectively to the nodal inertia, stiffness and damping. Translational and rotational inertia can be also allocated in each node for a better fit of the model.

In Eq. (1) is presented a generic rotor equation of motion, in the matrix form, obtained from the Lagrange equations.

$$\mathbf{M}\ddot{\mathbf{q}} + \mathbf{D}\dot{\mathbf{q}} + \mathbf{K}\mathbf{q} = \mathbf{f} \tag{1}$$

In this equation, $\mathbf{M}$ is the inertial matrix, $\mathbf{D}$ is the combination of the dumping ($\mathbf{C}$) and gyroscopic ($\mathbf{G}$) matrices (as presented in Eq. (2), where $\boldsymbol{\Omega}$ is the rotor rotational speed), $\mathbf{K}$ is the stiffness matrix, $\mathbf{q}$ is the nodal displacements (linear and angular) vector and $\mathbf{f}$ is the generalized forces vector. Each vector has a length of $4n$, as the size of each matrix is $4n \times 4n$, where n is the number of nodes.

$$\mathbf{D} = \mathbf{C} + \Omega\mathbf{G} \tag{2}$$

The assembly of the matrices presented in Eq. (1) and Eq. (2) is done through the analysis of the influence that each element of the system (shaft elements, disks and bearings) exerts on each node associated to its degrees of freedom.

It is important to highlight the bearings contribution, since some assumptions are considered about it. Because it is a FEM discretized model, each bearing acts in a node independently. As the point of reference is the point of action of forces, there are no moments. Considering the principle of virtual works, as presented by Lalanne and Ferraris (1998), the expressions for the force due to stiffness and damping of each bearing is given in Eq. (3), where $\mathbf{q}_b$ is the nodal displacement and $\mathbf{K}_b$ and $\mathbf{C}_b$ are, respectively, the bearing stiffness and damping matrices, given by Eq. (4) and Eq. (5).

$$\mathbf{f}_b = -\mathbf{K}_b\mathbf{q}_b - \mathbf{C}_b\dot{\mathbf{q}}_b \tag{3}$$

$$\mathbf{K}_b = \begin{bmatrix} k_{xx} & k_{xz} & 0 & 0 \\ k_{zx} & k_{zz} & 0 & 0 \\ 0 & 0 & 0 & 0 \\ 0 & 0 & 0 & 0 \end{bmatrix} \tag{4}$$

$$\mathbf{C}_b = \begin{bmatrix} c_{xx} & c_{xz} & 0 & 0 \\ c_{zx} & c_{zz} & 0 & 0 \\ 0 & 0 & 0 & 0 \\ 0 & 0 & 0 & 0 \end{bmatrix} \tag{5}$$

The matrices elements subscript with *xx* are related to the horizontal forces and the ones subscript with *zz* are related to vertical forces. Elements subscript with *xz* and *zx* are so called cross-terms, and will not be considered in the models, making $k_{xz} = k_{zx} = 0$ and $c_{xz} = c_{zx} = 0$. Also, the bearings will be considered isotropic for all models, so $k_{xx} = k_{zz}$ and $c_{xx} = c_{zz}$.

In another hand, the generalized forces vector can be analyzed in detail, since only unbalance will be considered in this case. In this way, the forces vector for each node can be defined as Eq. (6), where f_x and f_z are, respectively, the horizontal and vertical unbalance components, given by Eq. (7), where m_u is the unbalance mass, ε is the unbalance eccentricity and ϕ is the unbalance phase. The index *i* refers to the node where the unbalance forces act.

$$\mathbf{f}_i(t) = \begin{Bmatrix} f_x \\ f_z \\ 0 \\ 0 \end{Bmatrix}_i \tag{6}$$

$$\begin{cases} f_x = m_u\varepsilon\Omega^2\sin(\Omega t + \phi) \\ f_z = m_u\varepsilon\Omega^2\cos(\Omega t + \phi) \end{cases} \tag{7}$$

Will be considered in this work that there is no phase angle between the unbalance and the rotors displacement reference ($\phi = 0$). Also, the node where the unbalance is associated is considered previously known for each case, so the fault location is not addressed in this work.

In terms of a state-space problem, and considering Eq. (8), Eq. (1) can be presented as Eq. (9) in the form of a state system.

$$\begin{Bmatrix} \mathbf{x}_2 \\ \mathbf{x}_1 \end{Bmatrix} = \begin{Bmatrix} \dot{\mathbf{q}} \\ \mathbf{q} \end{Bmatrix} \tag{8}$$

$$\begin{cases} \mathbf{M}\,\dot{\mathbf{x}}_2 + \mathbf{D}\,\mathbf{x}_2 + \mathbf{K}\,\mathbf{x}_1 = \mathbf{f} \\ \dot{\mathbf{x}}_1 = \mathbf{x}_2 \end{cases} \tag{9}$$

However, as it is desired to estimate the system external forces, in this case, unbalance, and the vector **f** must be included in the state vector, augmenting the ordinary state-vector. Moreover, since the unbalance forces vary in time, there is a derivative. Therefore, considering eq. (7), the forces dynamics is given by eq. (10).

$$\begin{cases} \dot{f}_x = \Omega\, f_z \\ \dot{f}_x = -\Omega\, f_x \end{cases} \tag{10}$$

From Eq. (9), considering the unknown unbalance forces and the dynamics brought by Eq. (10), in order to solve the problem, it is formulated as a state-space problem where the state is a vector containing the generalized coordinates, their derivatives and the unknown forcing terms. The space-state system is present by Eq. (11).

$$\begin{cases} \mathbf{M}\,\dot{\mathbf{x}}_2 + \mathbf{D}\,\mathbf{x}_2 + \mathbf{K}\,\mathbf{x}_1 = \mathbf{f} \\ \dot{\mathbf{x}}_1 = \mathbf{x}_2 \\ \dot{\mathbf{f}} = \boldsymbol{\Psi}\,\mathbf{f} \end{cases} \tag{11}$$

The matrix $\boldsymbol{\Psi}$ is a square matrix with most terms equal to zero, excluding the ones related to the nodes where the unbalance acts. Eq. (12) gives the submatrix considered in this case. Once again, the index *i* refers to the node where the unbalance forces act.

$$\boldsymbol{\Psi}\left[i,\ldots,(i+3);i,\ldots,(i+3)\right] = \begin{bmatrix} 0 & \Omega & 0 & 0 \\ -\Omega & 0 & 0 & 0 \\ 0 & 0 & 0 & 0 \\ 0 & 0 & 0 & 0 \end{bmatrix} \tag{12}$$

With the forcing vector **f** as part of the estimation problem, it is considered a new forcing vector, obtained from the output of a linear filter driven by zero-mean Gaussian white noise. Besides that, Eq. (11) can be presented in the matrix form, as shown in Eq. (13).

$$\begin{Bmatrix} \dot{\mathbf{x}}_2 \\ \dot{\mathbf{x}}_1 \\ \dot{\mathbf{f}} \end{Bmatrix} = \begin{bmatrix} -\mathbf{D}\,\mathbf{M}^{-1} & -\mathbf{K}\,\mathbf{M}^{-1} & \mathbf{M}^{-1} \\ \mathbf{I}_{4n\times 4n} & \mathbf{0}_{4n\times 4n} & \mathbf{0}_{4n\times 4n} \\ \mathbf{0}_{4n\times 4n} & \mathbf{0}_{4n\times 4n} & \boldsymbol{\Psi}_{4n\times 4n} \end{bmatrix} \begin{Bmatrix} \mathbf{x}_2 \\ \mathbf{x}_1 \\ \mathbf{f} \end{Bmatrix} + \begin{bmatrix} \mathbf{M}^{-1} \\ \mathbf{0}_{4n\times 4n} \\ \mathbf{0}_{4n\times 4n} \end{bmatrix} w \tag{13}$$

The Gaussian white noise, *w*, is defined by Eq. (14), with covariance matrix **Q**.

$$w \in \mathbb{R}^{4n},\ w \sim N\left(0,\mathbf{Q}\right) \tag{14}$$

Equation (13) can be presented in a more compact way, as follows.

$$\dot{\mathbf{x}} = \mathbf{A}\,\mathbf{x} + \mathbf{B}\,w \tag{15}$$

Considering that the only measurements available are the horizontal and vertical displacements in a single node of each rotor, the observation equation for the augmented model can be presented. Measurements inherent errors can be modeled as zero-mean Gaussian noise with covariance matrix **R**, resulting in the observation equation, Eq. (16).

$$\mathbf{y} = \mathbf{H}\mathbf{x} + v \tag{16}$$

The measurements Gaussian noise, *v*, is defined by Eq. (17).

$$v \in \mathbb{R}^2,\ v \sim N\left(0, \mathbf{R}\right) \tag{17}$$

The matrix **H** is also a square matrix with most terms equal to zero, excluding the ones related to the node where the measurements are taken. Eq. (18) gives the submatrix considered in this case. In this case, the index *j* refers to the node where the displacements can be observed.

$$\mathbf{H}\left[j,...,\left(j+3\right);j,...,\left(j+3\right)\right] = \begin{bmatrix} 1\,0\,0\,0 \\ 0\,1\,0\,0 \\ 0\,0\,0\,0 \\ 0\,0\,0\,0 \end{bmatrix} \tag{18}$$

In this way, the rotor dynamic system in the form of state space equations is represented by Eq. (19).

$$\begin{cases} \dot{\mathbf{x}} = \mathbf{A}\,\mathbf{x} + \mathbf{B}\,w \\ \mathbf{y} = \mathbf{H}\mathbf{x} + v \end{cases} \tag{19}$$

As the states of the state-space evolve continuously, but the measurements are taken discreetly, with a sampling rate defined, the state-space representation is hybrid (continuous-discrete). For computational purposes, the continuous process model can be discretized, using the same sampling rate as used in the measurements.

In this case, it is interesting to note that the objective of the study is to estimate only the amount of unbalance. Considering that the vector sum of all different sources of unbalance presented in a rotating machinery can be combined into a single vector, this vector can represent an imaginary heavy spot on each rotor. Since the heavy spot is previously located and the rotational speed is known for every time instant (the experimental data were collect during a machine run up), the pair of equations in Eq. (7) can be simplified to a single time independent equation, presented in Eq. (20).

$$f_u\left(\Omega\right) = m_u \varepsilon\, \Omega^2 \tag{20}$$

In this way, the discretization steps will be defined by the number of rotational speeds in which the displacement amplitude of each rotor was observed. For each rotational speed, Ω_k, the state must be estimated. Thus, the discrete state-space model is represented by Eq. (21), below.

$$\begin{cases} \mathbf{x}_{k+1} = \mathbf{A}\,\mathbf{x}_k + \mathbf{B}\,w_k \\ \mathbf{y}_k = \mathbf{H}\mathbf{x}_k + v_k \end{cases} \tag{21}$$

Thus, the estimated state ($\hat{\mathbf{x}}$) propagation equation is given by Eq. (22) and the state covariance matrix (**P**) propagation given by Eq. (23). In these cases, the notation (-) represents the priori and the notation (+), the posteriori.

$$\hat{\mathbf{x}}_k^- = \mathbf{A}\,\hat{\mathbf{x}}_{k\text{-}1}^+ \tag{22}$$

$$\mathbf{P}_k^- = \mathbf{A}\,\mathbf{P}_{k-1}^+\mathbf{A}^T + \mathbf{C}\,\mathbf{Q}\,\mathbf{C}^T \tag{23}$$

In other hand, the update equations are given next: the Kalman gain matrix (**K**), given by Eq. (24), the covariance matrix update, given by Eq. (25) and the state update, given by Eq. (26).

$$\mathbf{K}_k = \mathbf{P}_k^-\,\mathbf{H}^T\left(\mathbf{H}\,\mathbf{P}_k^-\,\mathbf{H}^T + \mathbf{R}\right)^{-1} \tag{24}$$

$$\mathbf{P}_k^+ = \mathbf{P}_k^- - \mathbf{K}_k\,\mathbf{H}\,\mathbf{P}_k^- \tag{25}$$

$$\hat{\mathbf{x}}_k^+ = \mathbf{A}\,\hat{\mathbf{x}}_k^- + \mathbf{K}_k\left(\mathbf{y}_k - \mathbf{H}\,\hat{\mathbf{x}}_k^-\right) \tag{26}$$

It is important to highlight that the noise sequences, w and v, are considered mutually independent and uncorrelated, as a consequence of being Gaussian. The covariance matrices **Q**, for the state variables, and **R**, for the measurements, are admitted constant and diagonal.

3 ROTATING MACHINERY

As mentioned before, two rotating machinery were considered to apply the earlier described method: a laboratory test rig and an industrial turbocharger.

3.1 The Lab Test Rig

The test rig considered in this work was originally built in the Vibration and Acoustic Laboratory (LAVI) of COPPE/UFRJ (Abrantes and Michalski, 2002 and Michalski, 2004). The test rig can be described as a Jeffcott rotor, with the shaft and the disk made of steel SAE 1045, with a total length of 420 mm and a shaft diameter of 12 mm. The disk is fixed in the shaft center, equally distanced from each bearing, with a diameter of 150 mm and thickness of 15 mm. The bearings were manufactured in bronze with the inside diameter of 8,1 mm and the length of 8,0 mm. The radial clearance is about 0,1 mm. The rotor mass is about 1,47 kg.

In Fig. 1 is presented the discretized model of this rotor. The shaft is represented in blue, the disk in red and the bearings in green. The blue dot in the disk is the position of the imaginary heavy spot representing unbalance. This is a very simple discretized model, with only 5 nodes.

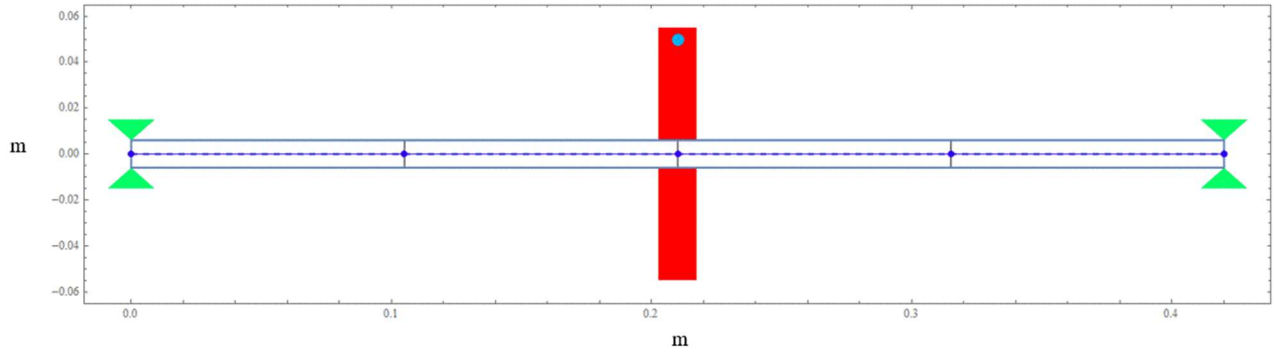

Figure 1: Test rig FE model.

The bearings stiffness coefficients, k_{xx} and k_{zz}, are equal, as mentioned before, have a considered nominal value of 5.10^4 N.m. On other hand, the damping coefficients, c_{xx} and c_{zz}, also equal, have a nominal value of 1.10^3 N.s/m. As proposed by Lalanne and Ferraris (1998), a single value for the entire speed range is considered for the bearings stiffness and damping coefficients.

The model first critical speed is around 51,15 Hz, or 3069 RPM. In the considering the operational range (2000-7000 RPM), the rotor just reaches one critical speed, and just the vibration first mode can be considered.

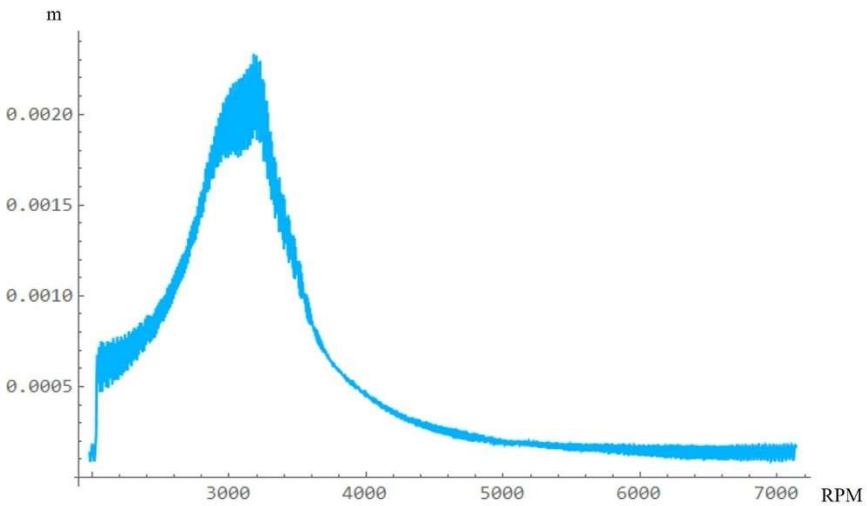

Figure 2: Test rig experimental data.

The displacement measurements are taken in the disk (node 3, in the presented model). Inductive analog probes are used to collect the data. In order to simplify the analysis, and considering Eq. (20), the displacements, measured at 45º and 135º in relation to the horizontal plane, are merged considering the square root of sum of squares. In Fig. 2 is presented the experimental data. The unbalanced applied during this run up is about 562,5 g.mm.

3.2 The Industrial Turbocharger

The industrial turbocharger considered in this work is actually used in the petrochemical industry. Due to industrial secrecy issues, there is not much information about the machine. However, it is known that the total length is about 159,75 mm and the rotor mass is about 246,5 kg. The first bearing is set up about 173 mm from the left end and the second bearing is set up about 227,75 mm from the right end.

In Fig. 3 is presented the discretized model of this rotor. As mentioned before, the shaft is represented in blue, the disks elements in red and the bearings in green. The blue dot in the left end is the position of the imaginary heavy spot representing unbalance. The red dots along the shaft center line are concentrated elements of inertia. This is a much more complex discretized model, compared to the test rig, with 87 nodes.

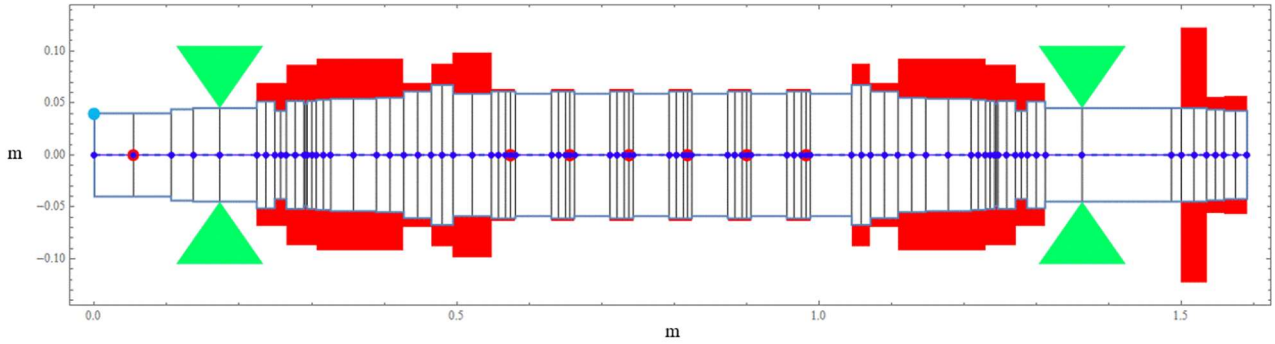

Figure 3: Turbocharger FE model.

The displacement measurements are taken in the two bearings (nodes 5 and 79, from the left to the right, in the presented model). However, just the measurements of the second bearing, node 79, will be used in this work. Also, inductive analog probes are used to collect the data displacements, measured at 45º and 135º in relation to the horizontal plane. The simplification mentioned before is considered again and the sensor data are merged considering the square root of sum of squares. In Fig. 4 is presented the experimental data, collect during the manufacturer's commissioning. The unbalanced applied during this run up was about 1700 g.mm.

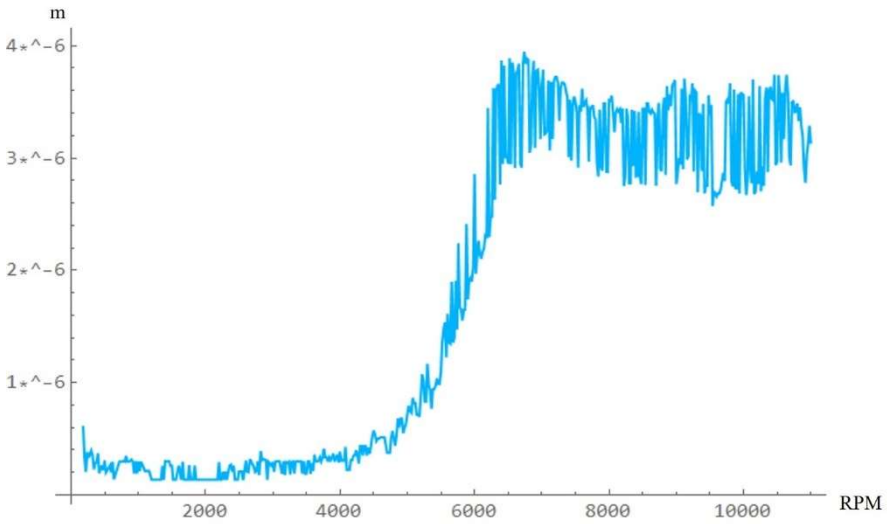

Figure 4: Turbocharger experimental data.

4 RESULTS AND DISCUSSION

In this section, some results will be presented and evaluated. Basically, three groups of results will be considered: first, the unbalance estimation using the models' data previously presented. Then, the unbalance estimation considering variations in the kick off value. And, finally, the unbalance estimation considering the bearings stiffness and damping uncertainties, with propagation.

A common consideration for all cases concerns the frequency range analyzed. As the unbalance is most noticeable near critical speeds and, in both machines considered, only a critical speed is achieved, the speed range will be limited to a value close to the critical speed of each machine. In this way, the unbalance value can be estimated more precisely.

4.1 Unbalance Estimation

Basically, the unbalance estimation is carried out considering the method presented in section 2, and the models and experimental data presented in section 3. Some previous considerations, however, must be taken in each case.

4.1.1 Test Rig

In this case, for the test rig, the process model noise covariance matrix is 50.**I**, the experimental data noise variance is $4{,}22.10^{-9}$ and the state estimation error covariance matrix, $\mathbf{P}_0$, is an identity matrix. All the initial state-vector values were zero, except for the unbalance force, with an amount of unbalance of 1250 g.mm.

In Fig. 5 is presented the estimates of the displacement, compared with the experimental data, and in Fig. 6 the unbalance amount estimation.

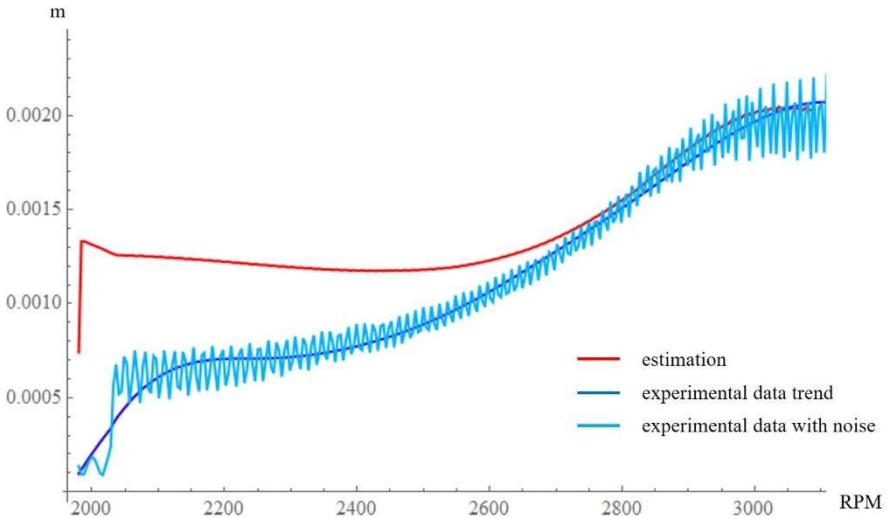

Figure 5: Test Rig Displacement Estimation.

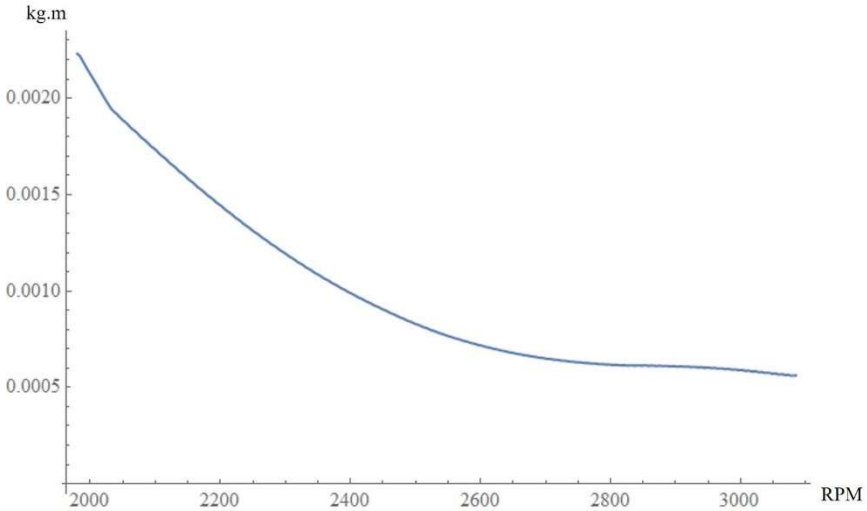

Figure 6: Test Rig Unbalance Estimation.

The estimated value for the unbalance amount was 562,37 g.mm. Considering the real value, 562,5 g.mm, the error was only 0,022%, that is, fully neglectable. It is interesting to note that, due to the signal noise magnitude, the state estimate values the model, generating a more filtered result.

4.1.2 Turbocharger

For the turbocharger, the process model noise covariance matrix is also 50.**I**, the experimental data noise variance is $7{,}07.10^{-14}$ and the state estimation error covariance matrix, $\mathbf{P}_0$, is 10.**I**. All the initial state-vector values were zero, except for the unbalance force, with an amount of unbalance of 2100 g.mm.

In Fig. 7 is presented the estimates of the displacement, compared with the experimental data, and in Fig. 8 the unbalance amount estimation.

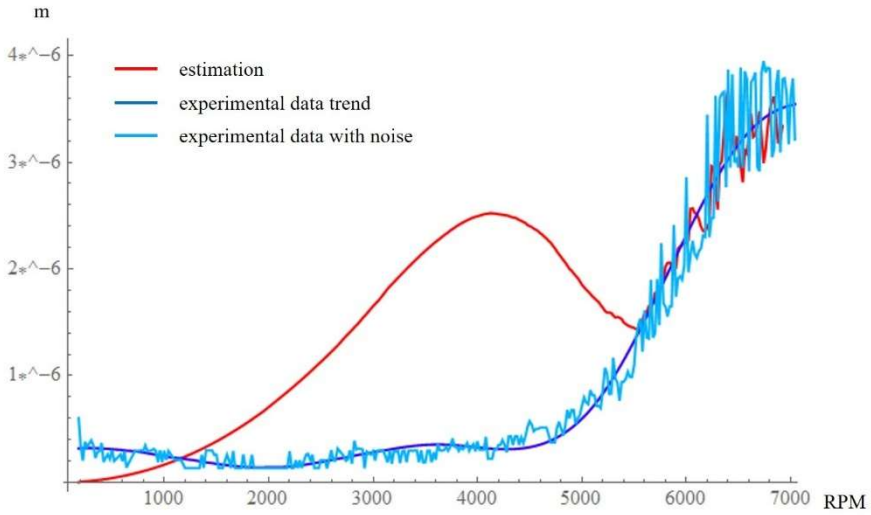

Figure 7: Turbocharger Displacement Estimation with Kickoff Value Variation

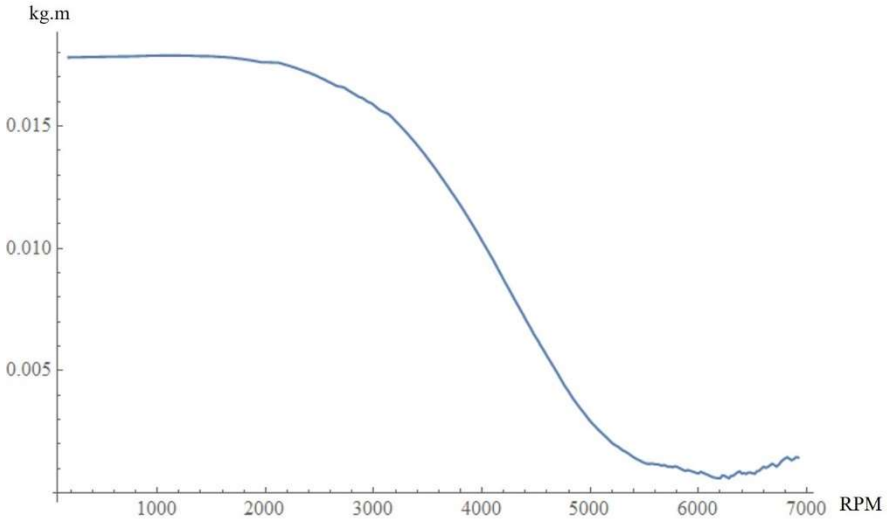

Figure 8: Turbocharger Unbalance Estimation.

In this case, the estimated value for the unbalance amount was 1440,62 g.mm. Considering the real value, 1700 g.mm, the error was 15,25%. Although it is a considerable deviation in the result, it is totally justifiable. In fact, unlike the test rig, the signal noise magnitude in this case is too small, and the state estimate values the measurements, generating a less filtered result. In fact, it is noticeable, especially considering the displacement, as the estimate is perfectly filtered initially, and as the filter begins to adjust to the measurements, its behavior changes, even "forgetting" the model.

4.2 Unbalance Estimation with Variation of the Initial Unbalance

In order to verify the method robustness, several estimates will be evaluated considering different initial values for the unbalance, the kick off. In this case, in addition to the Kalman filter, will be applied the Monte Carlo method. Were carried out fifty iterations, both for the test rig and the turbocharger model, with the amount of unbalance varying between 12,5 g.mm and 3725 g.mm for the first and between 21 g.mm and 6258 g.mm for the former. The other parameters (process model noise covariance matrix, experimental data noise variance and the state estimation error covariance matrix, $\mathbf{P}_0$) remain the same as the ones used in section 3.

4.2.1 Test Rig

In Fig. 9 are presented the estimates of the displacement, compared with the experimental data, and in Fig. 10 the unbalance amount estimation.

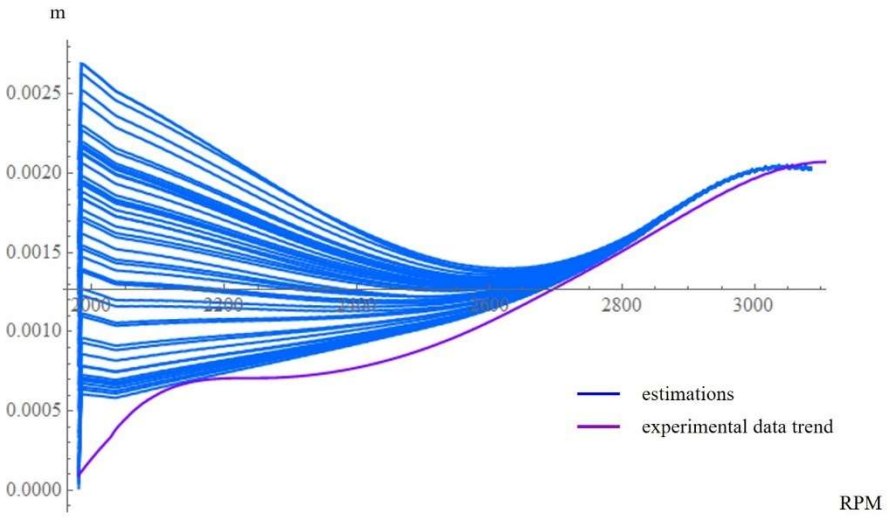

Figure 9: Test Rig Displacement Estimation with Kick off Variation.

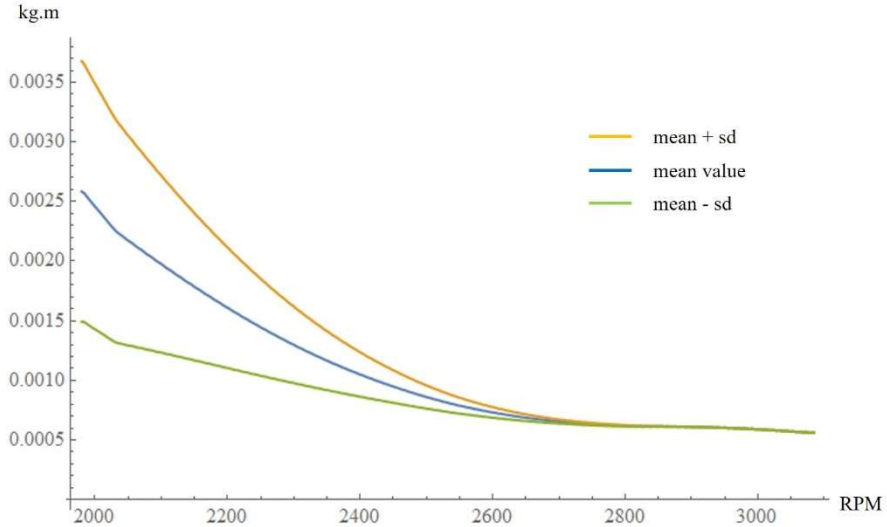

Figure 10: Test Rig Unbalance Estimation with Kick off Variation.

It is noticeable how robust the method can be, regarding to the kick off value. Even with significative differences in the filter initial behavior, convergence occurs and the state estimation is done without problems. The last estimated value for the unbalance amount was 562,13 g.mm. Considering the real value, 562,5 g.mm, the error was only 0,065%, and still fully neglectable.

Figure 11 presents a histogram with the unbalance estimates for each kick off value. Convergence by the mean is perfect, since the mean value and the last estimated value are the same. In this case, the standard deviation is 0,33 g.mm.

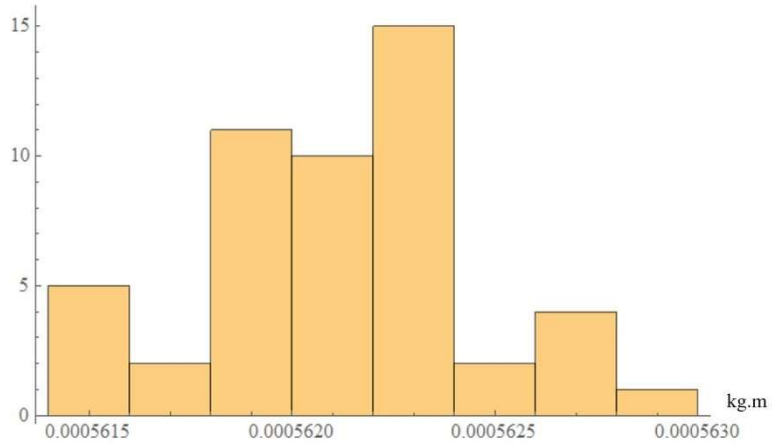

Figure 11: Test Rig Unbalance Estimation Histogram with Kick off Variation.

4.2.2 Turbocharger

In Fig. 12 are presented the estimates of the displacement, compared with the experimental data, and in Fig. 13 the unbalance amount estimation.

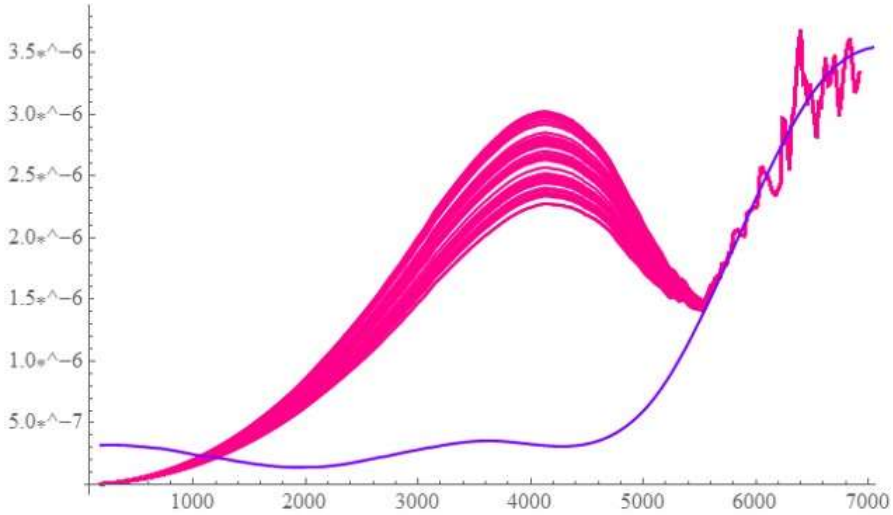

Figure 12: Turbocharger Displacement Estimation with Kick off Variation.

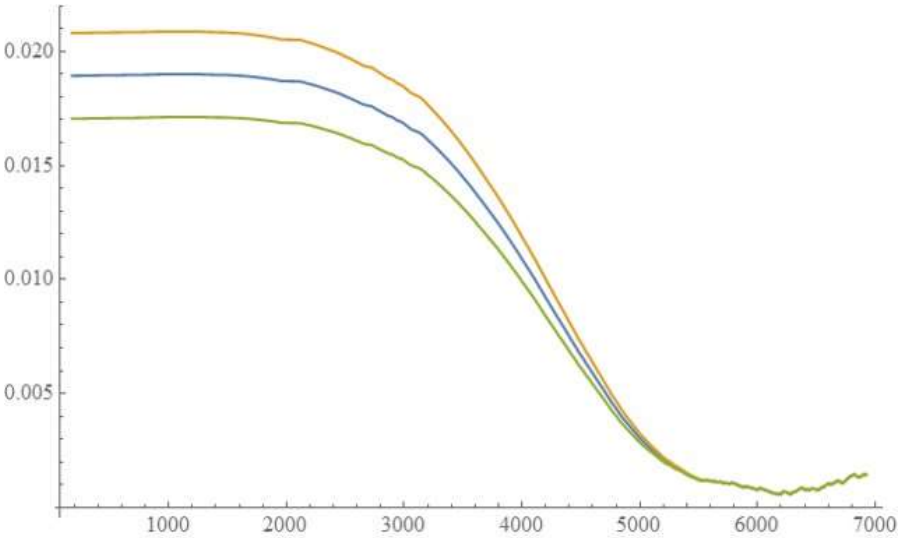

Figure 13: Turbocharger Unbalance Estimation with Kick off Variation.

Once again, the method can be presents to be very robust, regarding to the kick off value. The differences in the filter initial behavior were not so significant, but during its progression it is noticeable the influence of the initial value, until the estimates approach the experimental data and converge again without any problem. The last estimated value for the unbalance amount was 1440,55 g.mm. Considering the real value, 1700 g.mm, the error was 15,26%, considerable, but justifiable due to the small noise of the experimental data.

Figure 11 presents a histogram with the unbalance estimates for each kick off value. Again, convergence by the mean is perfect, since the mean value and the last estimated value are the same. The standard deviation is 0,19 g.mm in this case.

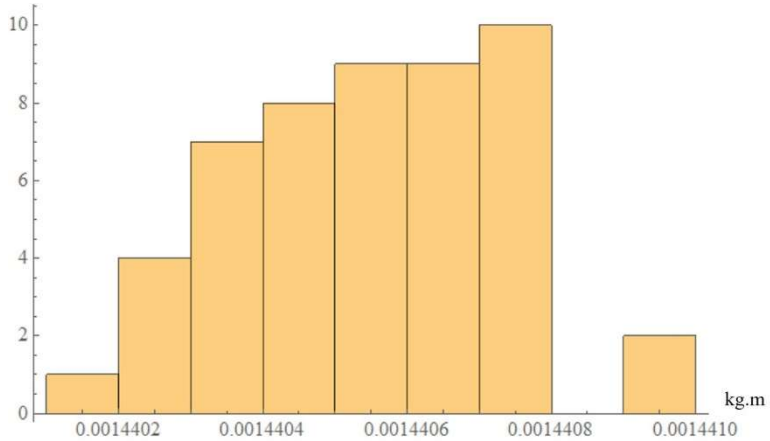

Figure 14: Turbocharger Unbalance Estimation Histogram with Kick off Variation.

4.3 Unbalance Estimation with Bearings' Stiffness and Damping Uncertainties Propagation

In this case, a similar process to the previous one is done, considering the Monte Carlo method and the Kalman Filter. However, instead of varying the unbalance initial value, the random variables will be the coefficients of stiffness and damping in both machines. The process model noise covariance matrix, experimental data noise variance and the state estimation error covariance matrix values still the same. Also, all the initial state-vector values were zero, except for the unbalance force, with an amount of unbalance of 1250 g.mm for the test rig and 2100 g.mm for the turbocharger.

4.3.1 Test Rig

In the test rig case, the bearings stiffness coefficients, k_{xx} and k_{zz}, and the damping coefficients, c_{xx} and c_{zz}, are considered random variables with uniform distribution. The bearing symmetry is kept, so $k_{xx} = k_{zz}$ and $c_{xx} = c_{zz}$. The stiffness coefficient range is between 3.10^4 N.m and 7.10^4 N.m. The damping coefficients range, on the other hand, is between 5.10^2 N.s/m and $1{,}5.10^3$ N.s/m. Considering the nominal value for each coefficient, the stiffness error can reach 40% and the damping error can reach 50%.

Next, in Fig. 15, are presented the estimates of the displacement, compared with the experimental data, and in Fig. 16 the unbalance amount estimation.

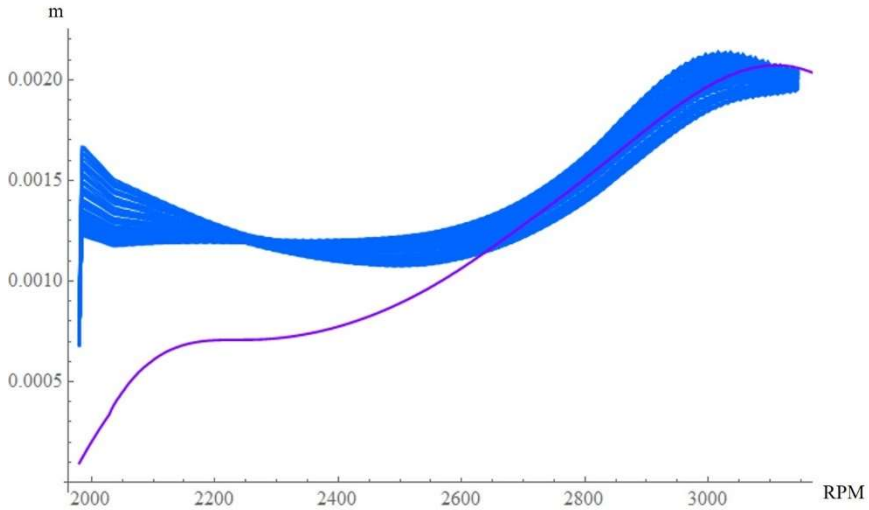

Figure 15: Test Rig Displacement Estimation with Stiffness and Damping Coefficients Variation.

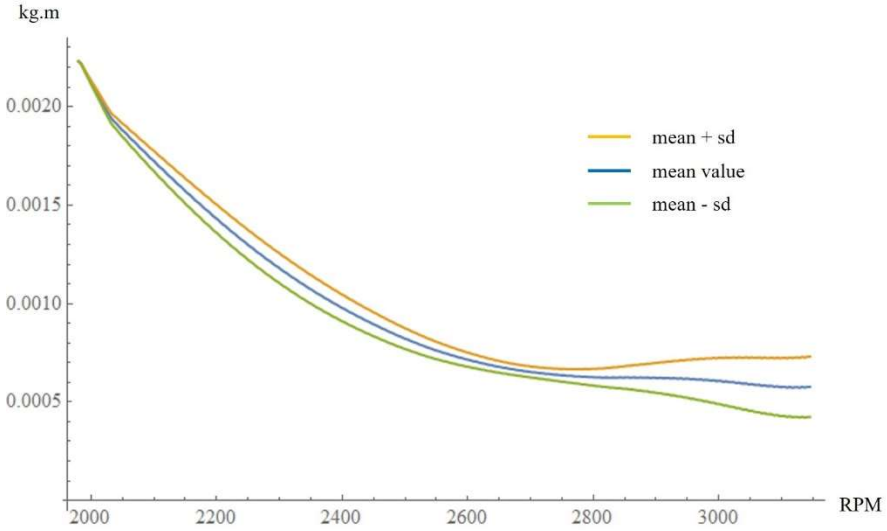

Figure 16: Test Rig Unbalance Estimation with Stiffness and Damping Coefficients Variation.

One hundred iterations have been made in this case. It is notorious how the displacement convergence goes without major problems. However, as it approaches the critical speed and the unbalance becomes more expressive, the error propagation from the coefficients for the final result becomes more significant. Although the mean value does not vary too much, the spread of the response increases.

The estimated value for the unbalance amount was 577,69 g.mm. Considering the real value, 562,5 g.mm, the error was 2,7%, and still very small.

Figure 17 presents a histogram with the unbalance estimates for each iteration. Convergence by the mean is, again, perfect, since the mean value and the last estimated value are the same. The standard deviation is 153,5 g.mm in this case.

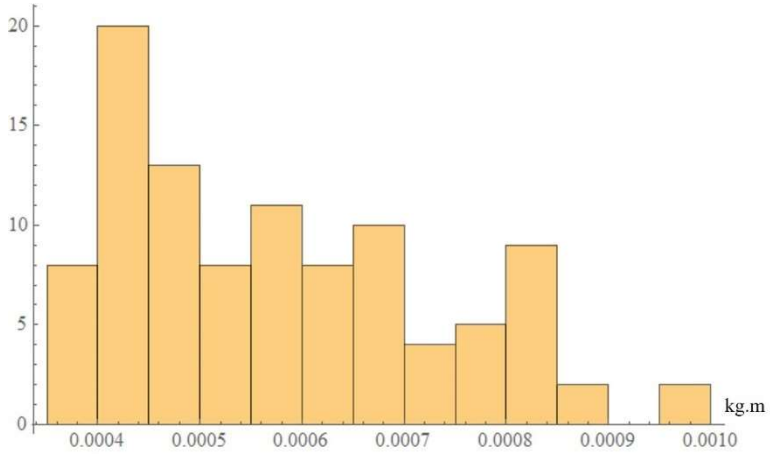

Figure 17: Test Rig Unbalance Estimation Histogram with Stiffness and Damping Coefficients Variation.

4.3.2 Turbocharger

In the turbocharge case, the bearings stiffness coefficients and damping coefficients are also considered random variables with uniform distribution. The bearing symmetry is kept, so $k_{xx} = k_{zz}$ and $c_{xx} = c_{zz}$. The stiffness coefficient range is between $1{,}55.10^8$ N.m and $1{,}95.10^8$ N.m, and the damping coefficients range is between $1{,}66.10^5$ N.s/m and $2{,}06.10^5$ N.s/m. Considering the nominal value for each coefficient, the stiffness error can reach 11,4% and the damping error can reach 10,75%, significantly lower percentage values than the previous case.

In Fig. 18 are presented the estimates of the displacement, compared with the experimental data, and in Fig. 19 the unbalance amount estimation.

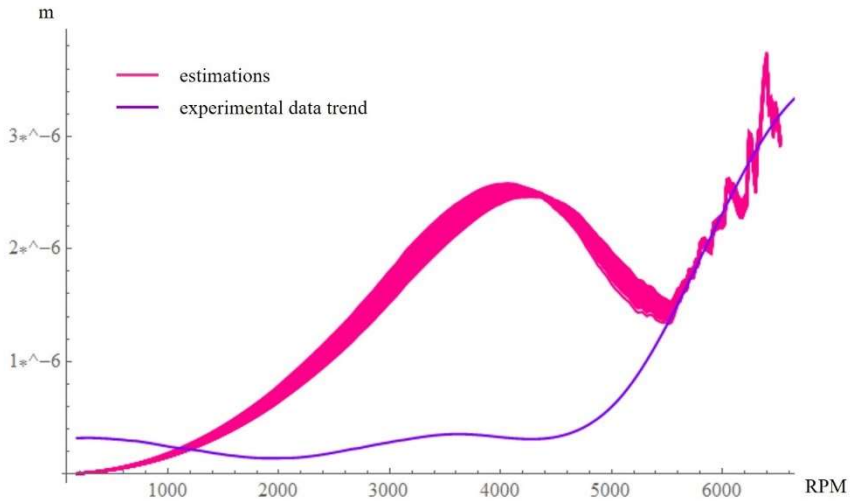

Figure 18: Turbocharger Displacement Estimation with Stiffness and Damping Coefficients Variation.

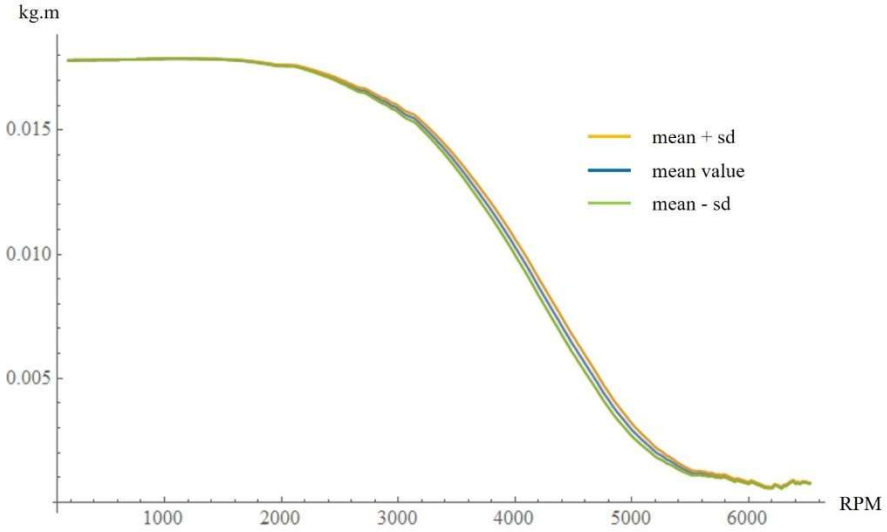

Figure 19: Test Rig Unbalance Estimation with Stiffness and Damping Coefficients Variation.

Fifty iterations have been made in this case. Both displacement and unbalance converge without any problem. Due to the small percentage variation of the bearing coefficients, both the displacement variation and the imbalance are also very small.

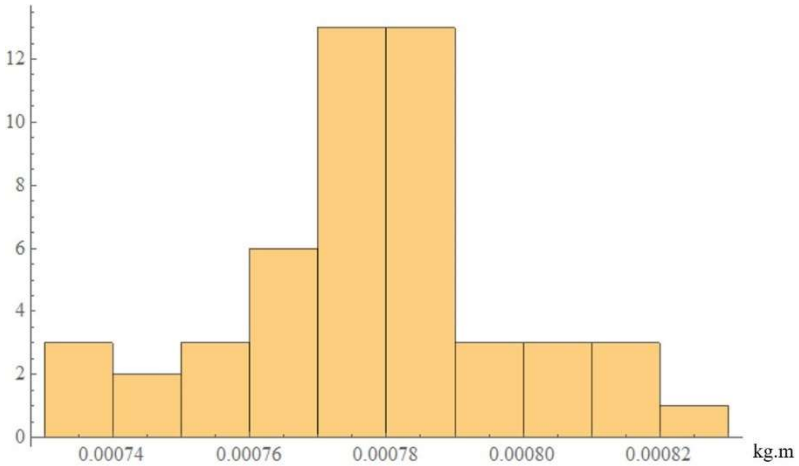

Figure 20: Turbocharger Unbalance Estimation Histogram with Stiffness and Damping Coefficients Variation.

Figure 20 presents a histogram with the unbalance estimates for each iteration. Convergence by the mean is, again, perfect, since the mean value and the last estimated value are the same. The estimated value for the unbalance amount was 778,24 g.mm. Considering the real value, 1700 g.mm, the error was 54,22%, and in this case, is a significantly high value, with the estimated value for the unbalance less than half of the actual value. The standard deviation is 204,29 g.mm in this case.

5 CONCLUSIONS

The objective of this paper was to present some initial results in the unbalance estimation in rotating machines using a Kalman Filter method. Two different machines, with very different characteristics, were analyzed. Both are horizontal rotors supported by two hydrodynamic bearings and just one critical speed in each rotational speed range. However, the similarities end there and the greatest difference between them is in the magnitude order of the measured response. In fact, it can be said that this difference defines what the "real world" is or not.

In both case the unbalance amount could be easily estimated. However, the algorithm behavior was completely different. The difference between what is desired to be estimated and the measures makes the filter behavior more sensitive. Moreover, with a measurement error so small, the filter disconsider the model from the moment it approaches convergence with the response. As a result, although the unbalance was estimated without major problems, the error in the case of the turbocharger is significantly higher than in the case of the test rig, although it is totally satisfactory.

Regarding robustness of the method, the obtained response can be considered excellent. Since the system parameters are known, significant variations in the kick off do not bring variations to the final response, considering the used data, both for the test rig and the turbocharger.

In other hand, once the method parameters are defined, variations in the system parameters brings different changes to the response of each considered machine. Regarding the test rig, there is no impact in the state estimate. Thus, even if the model has some errors, especially in the bearings coefficients, the unbalance estimation can still be performed. Regarding the turbocharger, although the state estimate is performed and the displacement error does not vary significantly graphically (comparing Fig. 7, Fig. 12 and Fig. 18), the unbalance amount error becomes very high. Apparently, the process of estimating system unbalance loses its tuning with the bearings parameters variation.

Next, in Tab. 1 and Tab. 2, a summary of the results obtained for both machines.

Table 1: Results Comparison – Test Rig.

Estimation Process	Unbalance Estimate	Estimate Error
Direct estimate	562,37 g.mm	0,022%
Estimative with kickoff variation	562,13 g.mm	0,065%
Estimative with bearing coefficients variation	577,69 g.mm	2,7%

Table 2: Results Comparison – Turbocharger.

Estimation Process	Unbalance Estimate	Estimate Error
Direct estimate	1440,62 g.mm	15,25%
Estimative with kickoff variation	1440,55 g.mm	15,26%
Estimative with bearing coefficients variation	778,24 g.mm	54,22%

It is noticeable that there is a significant increase in the unbalance estimate error in both cases, when the estimative is made considering bearings coefficients variations. However, in the test rig case, all the obtained results are very close to the real value. In fact, such a difference shows that, even in the case of an experimental test rig with its limitations, applying the methodology proposed with data collected in a controlled laboratory environment is simpler than applying the same methodology in real machine data. The process tuning depends, in fact, on the model, and knowing its parameters a priori becomes fundamental for the methodology successfully application.

Despite this, in conclusion, the work fulfills its objective as a first step. For future work, the estimation of other parameters, such as the phase and location of the unbalance, remains as a suggestion.

ACKNOWLEDGEMENTS

The authors would like to acknowledge CNPq for the financial support.

REFERENCES

Abrantes M. V. G. D.; Michalski, M. A. C., 2002, "Projeto e Construção de uma bancada Experimental para Estudos em Dinâmica de Rotores Horizontais", Final Project (Undergraduate Degree), Mechanical Engineering Department, Polytechnic School of Federal University of Rio de Janeiro, Rio de Janeiro, RJ, Brazil.

Bently, D. E.; Hatch, C. T, 2003, "Fundamentals of Rotating Machinery Diagnostics", 1st Edition, ASME Press (American Society of Mechanical Engineers).

Deepak Prabhakar, P.; Jagathy Raj V. P., 2014, "CBM, TPM, RCM and A-RCM - A Qualitative Comparison of Maintenance Management Strategies" in International Journal of Management & Business Studies – IJMBS, 4 (3): 49-56.

Haug, A. J., 2012, "Bayesian Estimation and Tracking: A Practical Guide", 1st edition, Wiley, John Wiley & Sons, Inc.

Lalanne, M.; Ferraris, G., 1998, "Rotordynamics Prediction in Engineering", 2nd Edition, John Wiley & Sons Ltd.

Lees, A. W.; Friswell, M. I., 2006, "Where Next for Condition Monitoring of Rotating Machinery?", in Advances in Vibration Engineering, 5 (4): 263-277.

Lees, A. W.; Sinha, J. K.; Friswell, M. I, 2009, "Model-based identification of rotating machines", in Mechanical Systems and Signal Processing, 23 (6): 1884-1893.

Michalski, M. A. C., 2004, "Análise Teórico Experimental do Comportamento Dinâmico de um Rotor Horizontal Suportado por Mancais Hidrodinâmicos", Dissertation (Master Degree), Mechanical Engineering Department, Polytechnic School of Federal University of Rio de Janeiro, Rio de Janeiro, RJ, Brazil.

Muszynska, A., 2005, "Rotordynamics", 1st edition, Taylor & Francis Group, Mechanical Engineering Series.

Rausand, M., 1998, "Reliability Centered Maintenance", in Reliability Engineering and System Safety, 60: 121-132.

Silva, C. W. (ed.), 2005, "Vibration and Shock Handbook", Taylor & Francis Group, Mechanical Engineering Series. Frank Kreith - Series Editor, Flórida, USA.

Sinha, J. K.; Lees, A. W.; Friswell, M. I., 2004, "Estimating unbalance and misalignment of a flexible rotating machine from a single run-down", in Journal of Sound and Vibration, 272 (2-3): 967-989.

Walker, R., Perinpanayagam, S., Jennions, I. K., 2013, "Rotordynamic Faults: Recent Advances in Diagnosis and Prognosis (Review Article)", in International Journal of Rotating Machinery, Hindawi Publishing Corporation, 2013.

RESPONSIBILITY NOTICE

The authors are the only responsible for the printed material included in this paper.